

Right-handed neutrino production through first-generation leptoquarks

Gokul Duraikandan,^{1,*} Rishabh Khanna,^{2,†} Tanumoy Mandal,^{1,‡} Subhadip Mitra,^{2,3,§} and Rachit Sharma^{1,¶}

¹Indian Institute of Science Education and Research Thiruvananthapuram, Vithura, Kerala, 695 551, India

²Center for Computational Natural Sciences and Bioinformatics,

International Institute of Information Technology, Hyderabad 500 032, India

³Center for Quantum Science and Technology, International Institute of Information Technology, Hyderabad 500 032, India

The collider phenomenology of leptoquarks (LQs) and right-handed neutrinos (RHNs) has been studied extensively in the literature. Because of the gauge singlet nature, the production of RHNs at the LHC is typically suppressed by the tiny light-heavy neutrino mixing angles. In this study, we explore a promising scenario where the presence of an LQ mediator significantly enhances RHN production. We focus on first-generation scalar and vector LQs interacting with the first-generation RHN. The prospects are better for the first-generation scenario than the other generations because of the enhanced parton distribution functions (PDFs) of first-generation quarks. The enhanced PDFs boost the production cross sections of LQs, particularly their single and indirect productions. Incorporating all production modes of LQs that result in a pair of RHNs, we estimate the discovery prospects by analysing the monoelectron and dielectron channels arising from the decay of the RHN pair. We find that the indirect production of LQs is crucial in determining the discovery reach at the HL-LHC for the first-generation scenario.

I. INTRODUCTION

Contemporary experimental advancements have established that at least two neutrino states possess tiny but nonzero masses (~ 0.1 eV). The type-I seesaw mechanism [1, 2] shows a simple way to generate the neutrino masses by introducing heavy right-handed neutrinos (RHNs) to the Standard Model (SM). However, the Majorana mass scale (Λ_M) of the RHNs must be very high—around the grand unification scale for Yukawa couplings of order unity—to make the light neutrinos sub-eV this way. Such a high mass scale renders the RHNs inaccessible at TeV-range colliders like the LHC. A Yukawa coupling of order 10^{-6} could bring Λ_M down to the TeV range, but, in that case, the RHNs would be long-lived and likely to decay outside detectors. The inverse seesaw mechanism (ISM) [3, 4] shows promise from the collider perspective, for it naturally contains TeV-scale RHNs that decay promptly, making them detectable at colliders.

Since RHNs are gauge singlets, the tiny light-heavy neutrino mixing angle severely suppresses their production at colliders. (Current constraints on the RHN mass and mixing angles are discussed in Ref. [5], while prospects for heavy RHN searches at future lepton colliders are discussed in Ref. [6].) An interesting possibility for RHN production arises from the decays of other beyond-the-SM particles, such as W' bosons [7–9], Z' bosons [10–18], or leptoquarks (LQs or ℓ_q) [19, 20], etc. Since, in these cases, the production is no longer dependent on the active-sterile mixing, they can be produced easily. From the LHC perspective, the production via TeV-scale LQs looks particularly promising [20].

LQs are hypothetical coloured bosons (scalar or vector) carrying both baryon and lepton numbers. Conse-

quently, they bridge the baryon and lepton sectors, enabling couplings between quarks and the RHNs. LQs naturally emerge in many extensions of the SM that aim to unify matter or forces. They are integral to a wide range of theoretical frameworks beyond the SM, such as the Pati-Salam model [21, 22], Grand Unified Theories [23, 24], composite models [25], coloured Zee-Babu models [26], technicolor models [27, 28] and Supersymmetry with R -parity violation [29], etc. Recently, LQs have garnered significant attention as potential explanations for various low-energy anomalies (see, e.g., Refs. [30–32]). Their collider phenomenology is also well-studied in the literature (e.g., Refs. [33–38]).

Previously, we studied the production of RHNs through second-generation LQs at the LHC [20]. Here, we focus on RHN productions via first-generation LQs. These LQs couple to a first-generation quark and the first-generation RHN, whose decay produces a first-generation lepton in the final state. In such a scenario, RHN pairs can be produced at the LHC through all LQ production mechanisms [20]: pair and single productions (P- and SPs), where the produced LQs decay to RHNs, and the indirect production (IP) [39] of a LQ, where a t -channel LQ exchange produces two RHNs ($pp \rightarrow \nu_R \nu_R$). For our collider study, we assume that a TeV-range first-generation LQ decays exclusively to a lighter first-generation RHN at the tree level, i.e., the branching ratio (BR) of the $\ell_q \rightarrow q \nu_R$ decay is essentially 100%. The nature of the LQ couplings strongly influences the SP and IP cross sections, as the quark parton distribution functions (PDFs) vary significantly across generations. As a result, the first-generation case requires a separate study from the second-generation one, even though the detection efficiencies of the first and second-generation leptons (i.e., e and μ) are not significantly different. However, the third-generation case differs from those two both in terms of initial-quark PDFs and final-state isolation/detection strategies. We plan to address the third-generation case in a separate study.

If a LQ decays predominantly to the RHN, it is not bound by any direct or indirect collider constraints—the LHC has yet to probe and constrain this part of the LQ parameter

arXiv:2412.19751v2 [hep-ph] 16 Jan 2025

* gokulduraikandan19@iisertvm.ac.in

† rishabh.khanna@research.iiit.ac.in

‡ tanumoy@iisertvm.ac.in

§ subhadip.mitra@iiit.ac.in

¶ rachit21@iisertvm.ac.in

TABLE I. List of LQs and their representations under the SM gauge groups. In the second column, we show the representations under $SU(3)_C$, $SU(2)_L$, and $U(1)_Y$, respectively. In the last column, we present the LQ interactions with ν_R [40].

LQ	$(SU(3)_C, SU(2)_L, U(1)_Y)$	Spin	Interaction Lagrangian
S_1	$(\bar{\mathbf{3}}, 1, 1/3)$	0	$y_{1ij}^{LL} \bar{Q}_L^{i,a} S_1 \varepsilon^{ab} L_L^{j,b} + y_{1ij}^{RR} \bar{u}_R^i S_1 e_R^j + \bar{y}_{1ij}^{RR} \bar{d}_R^i S_1 \nu_R^j + \text{h.c.}$
\bar{S}_1	$(\bar{\mathbf{3}}, 1, -2/3)$	0	$\bar{y}_{1ij}^{RR} \bar{u}_R^i \bar{S}_1 \nu_R^j + \text{h.c.}$
\tilde{R}_2	$(\mathbf{3}, 2, 1/6)$	0	$-\tilde{y}_{2ij}^{RL} \bar{d}_R^i \tilde{R}_2^a \varepsilon^{ab} L_L^{j,b} + \tilde{y}_{2ij}^{LR} \bar{Q}_L^{i,a} \tilde{R}_2^a \nu_R^j + \text{h.c.}$
U_1	$(\mathbf{3}, 1, 2/3)$	1	$x_{1ij}^{LL} \bar{Q}_L^{i,a} \gamma^\mu U_{1,\mu} L_L^{j,a} + x_{1ij}^{RR} \bar{d}_R^i \gamma^\mu U_{1,\mu} e_R^j + x_{1ij}^{RR} \bar{u}_R^i \gamma^\mu U_{1,\mu} \nu_R^j + \text{h.c.}$
\bar{U}_1	$(\bar{\mathbf{3}}, 2, -1/3)$	1	$\bar{x}_{1ij}^{RR} \bar{d}_R^i \gamma^\mu \bar{U}_{1,\mu} \nu_R^j + \text{h.c.}$
\tilde{V}_2	$(\bar{\mathbf{3}}, 1, -1/6)$	1	$\tilde{x}_{2ij}^{RL} \bar{u}_R^i \gamma^\mu \tilde{V}_{2,\mu}^b \varepsilon^{ab} L_L^{j,a} + \tilde{x}_{2ij}^{LR} \bar{Q}_L^{i,a} \gamma^\mu \varepsilon^{ab} \tilde{V}_{2,\mu}^b \nu_R^j + \text{h.c.}$

space. The RHN production through LQ decay becomes significant when neither of these particles is too heavy, and the RHN is lighter than the LQ. Since LQs are strongly interacting particles, they can be abundantly produced at the LHC, enhancing the RHN production. This process depends on a few parameters, such as the RHN and LQ masses, the RHN-LQ-quark couplings, and the PDFs of the initial partons. The cross section of the $qq \rightarrow \nu_R \nu_R$ process through a t -channel LQ exchange is proportional to the fourth power of the RHN-LQ-quark couplings. Hence, this coupling can not be small for the LQ-exchange process to be significant.

In this paper, we analyse RHN production through all the above-mentioned channels at the LHC. The plan of the paper is as follows. In the next section, we list the LQ models with RHN decay mode. In Section III, we discuss various possible final states arising from the decay of a pair of RHN that can be searched for at the High Luminosity-LHC (HL-LHC). We also discuss the SM backgrounds and selection criteria for the monoelectron and dielectron channels. We present our findings in Section IV and conclude in Section V.

II. LEPTOQUARK MODELS

We consider all possible LQs that simultaneously interact with a first-generation quark and a RHN. Table I lists the scalar and vector LQs (sLQs and vLQs) with the necessary couplings. Since we are only interested in the collider phenomenology of these models, we ignore the diquark operators to bypass the proton-decay restrictions. Following Ref. [40], we denote the Yukawa coupling matrices of sLQs and vLQs with quark-lepton pairs generically as y and x , respectively. The first subscript of the couplings indicates the $SU(2)_L$ representation and the superscripts indicate the chiralities of the fermions (the first one denotes the quark chirality and the second one, the lepton chirality). For simplicity, we assume both the Pontecorvo-Maki-Nakagawa-Sakata (PMNS) neutrino-mixing and the Cabibbo-Kobayashi-Maskawa (CKM) quark-mixing matrices to be approximately identity. This is justified since,

unlike the second-generation case [20], the cross sections of the processes initiated by the first-generation quarks are not affected significantly by the presence of the small off-diagonal terms in the quark-mixing matrix, and the LHC experiments cannot identify the flavour of the missing neutrinos. Vector LQs can have an extra gluon coupling allowed by the gauge symmetries that can affect their productions at the LHC [41, 42]:

$$\mathcal{L} \supset -ig_s(1 - \kappa) \chi_\mu^\dagger T^a \chi_\nu G^{a\mu\nu}, \quad (1)$$

where χ_μ denotes a generic vLQ and $G^{a\mu\nu}$ denotes the field strength tensor of the gluon.

III. LHC PHENOMENOLOGY

We incorporate the new physics Lagrangian in FEYNRULES [43] to produce the model files for further simulation. We use MADGRAPH5 [44] to generate the leading-order signal and background events with the NNPDF23LO1 [45] PDF set using the default dynamical scale setting. Where available, we use appropriate K_{QCD} factors to account for higher-order cross sections. In the signal, we use an average NLO K_{QCD} factor of 1.58 [46–51] for the sLQ pair production. The events are passed through PYTHIA8 [52] (for hadronization and showering) and DELPHES3 [53] (for detector simulation using the standard CMS card). We use FASTJET's anti-clustering algorithm [54, 55] to reconstruct the jets from the DELPHES tower objects. In our study, we use jets with two radii: (a) jets with $R = 0.4$ (we call this an AK4 jet and denote it as j) and (b) fatjet with $R = 1.2$ (denoted by J). We denote charged leptons with $\ell = \{e, \mu, \tau\}$.

A. Production at the LHC

LQs can be pair-produced via QCD or QED interactions alone, a mixture of QCD-QED interactions [39], or the RHN-LQ-quark interactions (parametrised by the couplings, x and y). Similarly, a single LQ can be produced

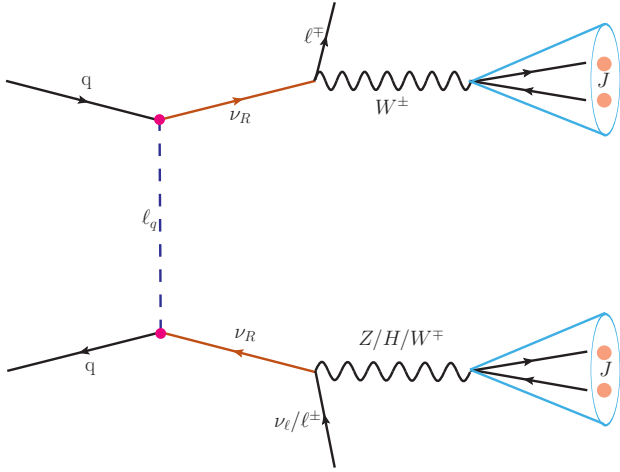


FIG. 1. Mono- and di-lepton final states from RHN pair production through a t -channel LQ exchange at the LHC.

in association with a RHN through x or y . In IP, a LQ is exchanged in the t -channel, producing two RHNs from two quarks (see Fig. 1). In the high-mass region, this nonresonant t -channel production of LQs surpasses their resonant productions when the new coupling(s) involved is(are) sufficiently large. While the PP is largely insensitive to the new couplings (as long as they are not too large), the SP and IP cross sections scale as their second and fourth powers, respectively (see Fig. 2). Because of relatively larger PDFs of the first-generation quarks, the IP is more significant for first-generation LQs than the second-generation ones [20].

In this analysis, we focus on first-generation LQs with $M_{\ell q} > M_{\nu_R}$, allowing them to decay into the first-generation RHN and a jet. As mentioned earlier, we assume this decay to be exclusive, i.e., the $\text{BR}(\ell_q \rightarrow \nu_R q) = 100\%$. All three production modes of LQs can produce a

TABLE II. Higher-order cross sections of the major background processes without decay and any cut. Their QCD orders are shown in the last column. We use these cross sections to compute the K factors to incorporate the higher-order effects.

Background processes		σ (pb)	QCD order
V + jets [56, 57]	Z + jets	6.33×10^4	$N^2\text{LO}$
	W + jets	1.95×10^5	NLO
VV + jets [58]	WW + jets	124.31	NLO
	WZ + jets	51.82	NLO
	ZZ + jets	17.72	NLO
Single t [59]	tW	83.10	$N^2\text{LO}$
	tb	248.00	$N^2\text{LO}$
	tj	12.35	$N^2\text{LO}$
tt [60]	tt + jets	988.57	$N^3\text{LO}$
ttV [61]	ttZ	1.05	$\text{NLO} + N^2\text{LL}$
	ttW	0.65	$\text{NLO} + N^2\text{LL}$

pair of RHNs accompanied by jets (from LQ decays or radiations). We further assume that the RHN mass is about a few hundred GeV, allowing it to decay resonantly through the $W + e$, $Z + \nu_e$, and $H + \nu_e$ channels (with BRs approximately in 2 : 1 : 1 proportion). Based on how the ν_R pair decays, we categorise the final states as follows.

Monoelectron: For the final state to have only one electron and no other charged lepton, one ν_R has to decay via the $W + e$ channel and the other one to $Z + \nu_e$ or $H + \nu_e$ channels where the Z/H boson decays hadronically (which can produce a fatjet). The various production channels contributing to monoelectron final states are as follows (see Fig. 1):

$$pp \rightarrow \left\{ \begin{array}{l} \ell_q \ell_q \\ \ell_q \nu_R (+j) \\ \nu_R \nu_R (+j) \end{array} \right\} \rightarrow \left\{ \begin{array}{l} (j \nu_R)(j \nu_R) \\ (j \nu_R) \nu_R (+j) \\ \nu_R \nu_R (+j) \end{array} \right\} \\ \rightarrow (e^\pm W_h^\mp)(\nu_e Z_h/H_h) + \text{jet(s)},$$

with the ν_e leading to missing transverse energy (MET). The field subscripts (except for ℓ_q and $\nu_{L/R}$) indicate decay modes; for example, h implies hadronic decay. The most dominant channel has a pair of RHN decaying as $\nu_R \nu_R \rightarrow (e^\pm W_h^\mp)(\nu_e Z_h/H_h)$, with an overall BR of about 23%. The second most dominant channel, $\nu_R \nu_R \rightarrow (e^\pm W_h^\mp)(\nu_e Z_{\nu_e})$, has a BR of about 7%. However, its contribution to our final results is minimal due to the low selection efficiency. All other channels with $\text{BR} \lesssim 1\%$ have a negligible impact on the results.

Dielectron: An electron-positron pair (e^+e^-) is produced when both RHNs decay via the $W + e$ channel. The final state with an e^-e^+ pair and no other charged lepton does not involve MET, making it fully reconstructible. The hadronic decays of the two W bosons can result in two fatjets. The various production channels contributing to dielectron final states are as follows:

$$pp \rightarrow \left\{ \begin{array}{l} \ell_q \ell_q \\ \ell_q \nu_R (+j) \\ \nu_R \nu_R (+j) \end{array} \right\} \rightarrow \left\{ \begin{array}{l} (j \nu_R)(j \nu_R) \\ (j \nu_R) \nu_R (+j) \\ \nu_R \nu_R (+j) \end{array} \right\} \\ \rightarrow e^\pm W_h^\mp e^\mp W_h^\pm + \text{jet(s)}.$$

In the dielectron channel, the dominant decay chain is $\nu_R \nu_R \rightarrow (e^\pm W_h)(e^\mp W_h)$, with an overall BR of 22%. Other channels, such as $\nu_R \nu_R \rightarrow (\nu_e Z_h/H_h)(\nu_e Z_e)$, have BRs of the order of 1%, and contribute negligibly to the results. A Z -veto to suppress the Drell-Yan dilepton background effectively eliminates the contribution from these subdominant processes. Consequently, we focus on the most dominant signals.

There are existing searches for dilepton final states via RHNs [11–13, 62, 63]. These studies are primarily motivated by Type-I seesaw models, where the RHNs are fully Majorana-type fermions leading to same-sign dilepton final states with lepton number violation. In contrast, we rely on the framework of inverse seesaw mechanism, where RHNs are pseudo-Dirac in nature, resulting in opposite-sign dilepton final states.

Trilepton: Trilepton final states through RHN decays can arise via the decay of a heavy neutral gauge boson or a

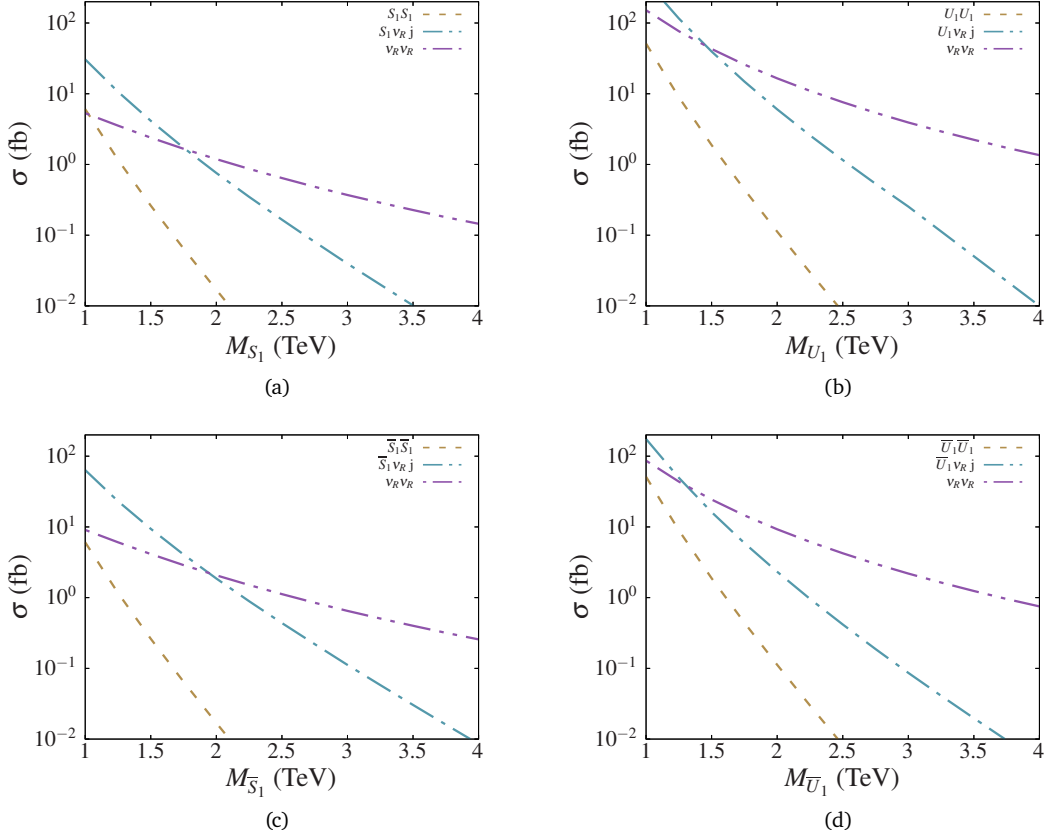


FIG. 2. Cross sections of direct and indirect production modes of charge-2/3 and 1/3 sLQs (left) and vLQs (right) at the 14 TeV LHC. For these plots, we set $M_{V_R} = 500$ GeV and $x, y = 1$. The vLQ plots are obtained for $\kappa = 1$.

TABLE III. Selection cuts applied on the monoelectron and dielectron final states.

Selection Cuts	Channels	
	Monoelectron	Dielectron
C1	$p_T(e) > 250$ GeV $p_T(j_1), p_T(j_2) > 110$ GeV	$p_T(e) > 120$ GeV No b -tagged jet
C2	$p_T(J_1) > 350$ GeV, $\eta(J_1) < 2.5$ $0.03 < \tau_{21}(J_1) < 0.4$	$p_T(J_1) > 280$ GeV, $\eta(J_1) < 2.5$
C3		$M(e_1, e_2) > 250$ GeV $M(J_1, e_1) > 450$ GeV
C4	$\cancel{E}_T > 180$ GeV $S_T > 900$ GeV	$S_T > 1200$ GeV

scalar. Both symmetric and asymmetric decay of the RHN pair can lead to the trilepton signal. The production and decay processes leading to these final states are as follows:

$$\begin{aligned}
 pp \rightarrow \left\{ \begin{array}{l} \ell_q \ell_q \\ \ell_q \nu_R (+j) \\ \nu_R \nu_R (+j) \end{array} \right\} &\rightarrow \left\{ \begin{array}{l} (j \nu_R)(j \nu_R) \\ (j \nu_R) \nu_R (+j) \\ \nu_R \nu_R (+j) \end{array} \right\} \\
 &\rightarrow \left\{ \begin{array}{l} (e^\pm W_\ell^\mp)(e^\pm W_h^\pm) + \text{jet}(s) \\ (e^\pm W_h^\mp)(\nu_e Z \ell) + \text{jet}(s) \end{array} \right\}.
 \end{aligned}$$

Even if we consider the RHN to be first generation, a leptonically decaying vector boson can decay to a μ or a τ lepton to produce a (mixed-flavour) trilepton final state. Trilepton channels have been explored in detail in Refs. [64–66].

Quadlepton: A pair of RHNs can also decay to give four-

TABLE IV. Cutflow for various background and signal contributions in the monoelectron and dielectron final states. We present the number of events surviving the cuts in Table III for the HL-LHC (14 TeV, 3 ab^{-1} ; in parentheses, we show the corresponding numbers for νLQs). Two benchmark points are considered to highlight the dominance of LQ IP at higher LQ masses.

Monoelectron final state	Selection Cuts			
	C1	C2	C3	C4
Signal benchmarks				
$M_{S_1(U_1)} = 1500 \text{ GeV}, M_{V_R} = 500 \text{ GeV}$ (LQ PP)	30 (160)	28 (148)	28 (148)	22 (119)
$M_{S_1(U_1)} = 1500 \text{ GeV}, M_{V_R} = 500 \text{ GeV}$ (LQ SP)	511 (4613)	471 (4230)	471 (4230)	334 (3244)
$M_{S_1(U_1)} = 1500 \text{ GeV}, M_{V_R} = 500 \text{ GeV}$ (LQ IP)	184 (3209)	133 (2292)	133 (2292)	82 (1437)
	Total number of signal events:			438 (4800)
$M_{S_1(U_1)} = 2500 \text{ GeV}, M_{V_R} = 500 \text{ GeV}$ (LQ PP)	< 1 (< 1)	< 1 (< 1)	< 1 (< 1)	< 1 (< 1)
$M_{S_1(U_1)} = 2500 \text{ GeV}, M_{V_R} = 500 \text{ GeV}$ (LQ SP)	17 (116)	16 (111)	16 (111)	12 (89)
$M_{S_1(U_1)} = 2500 \text{ GeV}, M_{V_R} = 500 \text{ GeV}$ (LQ IP)	50 (561)	36 (416)	36 (416)	24 (285)
	Total number of signal events:			36 (374)
Background processes				
$W_e(+2j)$	1.744×10^6	1.01×10^6	1.01×10^6	175326
$t_e t_h(+2j)$	387878	302625	30262	50557
$W_e W_j(+2j)$	30830	22383	22383	5791
$W_e Z_h(+2j)$	14474	10889	10889	2382
$t_e W_h + t_h W_e$	38503	22787	22787	2258
$t_e b$	6849	5502	5502	831
$t_e j$	161	131	131	21
	Total number of background events:			237166
Dielectron final state	Selection Cuts			
	C1	C2	C3	C4
Signal benchmarks				
$M_{S_1(U_1)} = 1500 \text{ GeV}, M_{V_R} = 500 \text{ GeV}$ (LQ PP)	15 (136)	15 (136)	13 (125)	13 (125)
$M_{S_1(U_1)} = 1500 \text{ GeV}, M_{V_R} = 500 \text{ GeV}$ (LQ SP)	285 (2768)	284 (2764)	230 (2522)	228 (2516)
$M_{S_1(U_1)} = 1500 \text{ GeV}, M_{V_R} = 500 \text{ GeV}$ (LQ IP)	182 (2478)	177 (2317)	150 (2016)	117 (1518)
	Total number of signal events:			358 (4159)
$M_{S_1(U_1)} = 2500 \text{ GeV}, M_{V_R} = 500 \text{ GeV}$ (LQ PP)	< 1 (< 1)	< 1 (< 1)	< 1 (< 1)	< 1 (< 1)
$M_{S_1(U_1)} = 2500 \text{ GeV}, M_{V_R} = 500 \text{ GeV}$ (LQ SP)	11 (91)	11 (91)	9 (86)	9 (86)
$M_{S_1(U_1)} = 2500 \text{ GeV}, M_{V_R} = 500 \text{ GeV}$ (LQ IP)	40 (441)	38 (423)	33 (372)	26 (310)
	Total number of signal events:			35 (396)
Background processes				
$(Z/\gamma^*)_e(+2j)$	253822	98786	51136	9065
$t_e t_e(+2j)$	23964	10523	6301	622
$W_e W_e(+2j)$	6159	3216	1909	494
$W_h Z_e(+2j)$	772	519	324	138
$t_e W_e$	2276	981	470	83
$Z_e Z_h(+2j)$	130	63	32	8
	Total number of background events:			10410

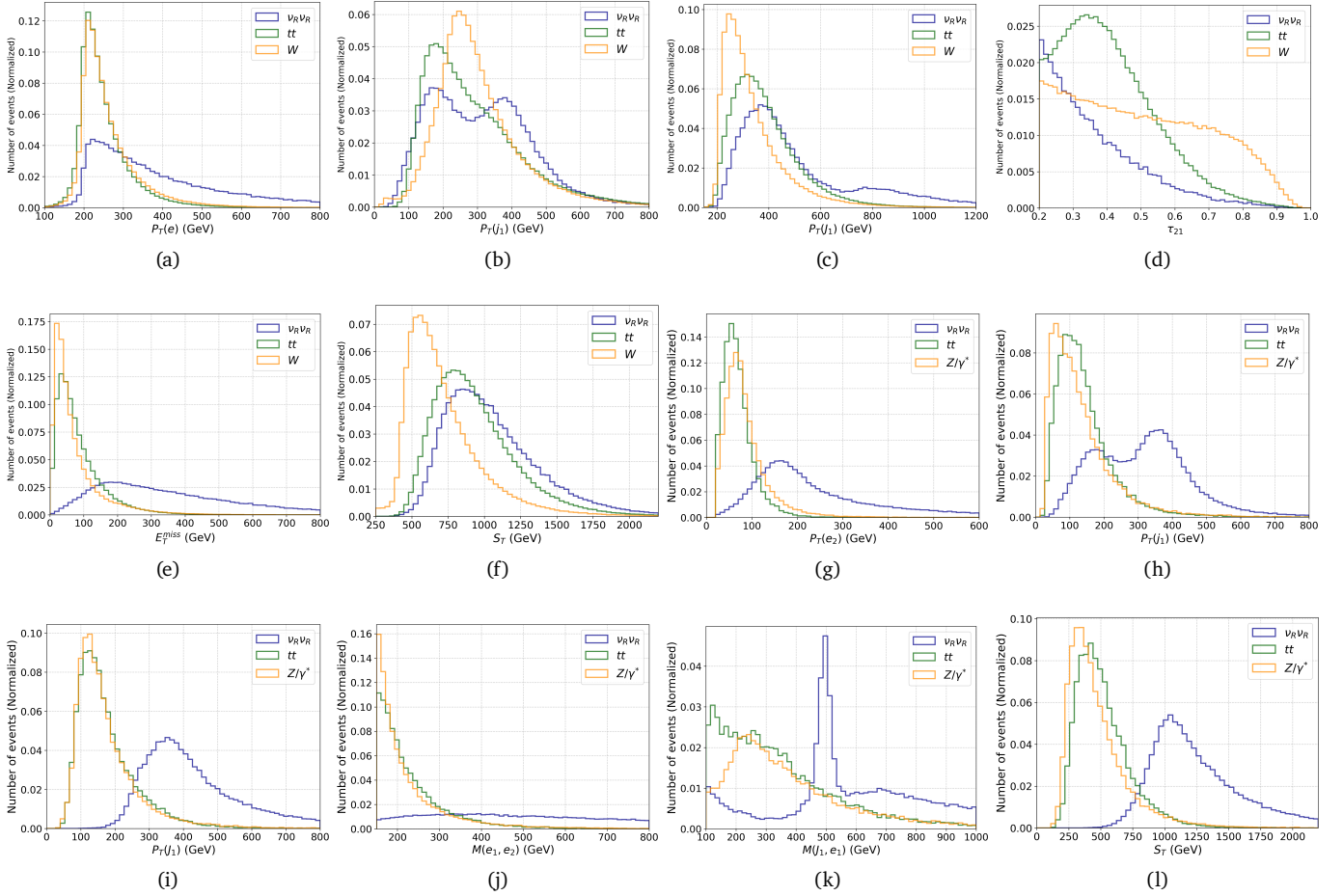


FIG. 3. Normalised distributions of kinematic variables for the signal and two dominant backgrounds in monoelectron [(a)–(f)] and dielectron [(g)–(l)] final states. The signal benchmark is $(M_{U_1}, M_{V_R}) = (2.5 \text{ TeV}, 0.5 \text{ TeV})$. For monoelectron, the dominant backgrounds are W_e and $t_e t_h$ and for dielectron, they are $(Z/\gamma^*)_e$ and $t_e t_e$. This distributions are obtained after applying the following cuts at the parton level: for monoelectron $p_T(e) > 200 \text{ GeV}$ and for dielectron $M(e_1, e_2) > 150 \text{ GeV}$.

TABLE V. Model-independent (i.e., from QCD-driven PP contributions obtained by taking $x \rightarrow 0$) mass limits on vLQs in GeVs for two different κ values. These numbers are obtained for the HL-LHC.

vLQ	Monoelectron				Dielectron			
	$\kappa = 1$		$\kappa = 0$		$\kappa = 1$		$\kappa = 0$	
	5σ	2σ	5σ	2σ	5σ	2σ	5σ	2σ
U_1	1160	1190	1315	1450	1269	1373	1553	1697
\bar{U}_1	1160	1190	1315	1450	1269	1373	1553	1697
\tilde{V}_2	1185	1300	1400	1622	1346	1537	1651	1833

lepton final states as:

$$\begin{aligned}
 PP \rightarrow \left\{ \begin{array}{l} \ell_q \ell_q \\ \ell_q \nu_R (+j) \\ \nu_R \nu_R (+j) \end{array} \right\} &\rightarrow \left\{ \begin{array}{l} (j\nu_R)(j\nu_R) \\ (j\nu_R)\nu_R (+j) \\ \nu_R \nu_R (+j) \end{array} \right\} \\
 &\rightarrow \left\{ \begin{array}{l} e^\pm W_\ell^\mp e^\mp W_\ell^\pm + \text{jet}(s) \\ \nu_e Z \ell \nu_e Z + \text{jet}(s) \end{array} \right\}.
 \end{aligned}$$

This channel suffers from the small leptonic BRs of the heavy bosons. However, it might still be accessible at the HL-LHC since the four-lepton SM background is small.

Similar channels have been analysed in the context of a $U(1)_{B-L}$ model in Ref. [67].

Displaced vertex: The RHN can exhibit a displaced vertex signature if its decay width is sufficiently small. In that case, the search strategy will differ significantly from that for prompt decays. The decay width of the RHN depends on its mass and the angle of mixing with its lighter counterpart. Displaced vertex signatures have been studied in Refs. [68–70] in the context of $Z' \rightarrow \nu_R \nu_R$ decay and in Refs. [71, 72] in the context of $\phi \rightarrow \nu_R \nu_R$ decay.

In extreme scenarios, the decay width of the RHN may become so small that it decays outside the detector, leading to missing energy in the event. Such cases require a separate analysis tailored to identifying missing energy signals.

Fatjet with MET: There are also nonleptonic final states involving one or more fatjets accompanied by some MET as follows.

$$pp \rightarrow \left\{ \begin{array}{l} \ell_q \ell_q \\ \ell_q \nu_R (+j) \\ \nu_R \nu_R (+j) \end{array} \right\} \rightarrow \left\{ \begin{array}{l} (j\nu_R)(j\nu_R) \\ (j\nu_R)\nu_R (+j) \\ \nu_R \nu_R (+j) \end{array} \right\} \\ \rightarrow (\nu_e Z_h/H_h)(\nu_e Z_h/H_h) + \text{jet}(s).$$

The background for this signal is expected to be very large. However, the signal can still be separable using advanced jet-substructure variables and machine-learning techniques. Similar final states have been analysed in the context of the inert Higgs doublet model in Ref. [73].

B. Signal, background and selection criteria

In this paper, we focus on the monoelectron and dielectron final states. We require at least two AK4 jets and a fatjet in the monoelectron channel, and two electrons and at least one fatjet in the dielectron channel. The relevant SM backgrounds and their cross sections are listed in Table II. Table III summarises the cuts applied to isolate the signals from the backgrounds. These are decided from the signal and background kinematic distributions, some of which are shown in Fig. 3. We show the cut-flows (the number of signal and background events surviving the cuts) for two benchmark points in the monoelectron and dielectron channels in Table IV. For a fixed RHN mass, increasing the LQ mass enhances the importance of its IP, which contributes more to the total signal events than the combined contributions of the PP and SP.

The dominant SM background for monoelectron and dielectron final states are $W_e + \text{jets}$ and $(Z/\gamma^*)_e + \text{jets}$, respectively, owing to their large cross-sections. Selection cuts try to suppress these contributions significantly while retaining a substantial fraction of the signal events. Consequently, the cuts are optimised to maximise event captures from the t -channel LQ exchange process. (The selection cuts used in this study differ slightly from those applied in Ref. [20], which focused on RHN production via second-generation LQs. This difference arises mainly because the t -channel LQ exchange plays a more significant role than the PP and the SP for first-generation LQs than the second-generation ones.) The next most significant background (for both channels) is $tt + \text{jets}$. As long as the signal contains no b jets, a b veto can tame it. In the monoelectron channel, a significant contribution comes from the $\nu_R \rightarrow H\nu_e \rightarrow bb\nu_e$ decay. Hence, we impose a b veto only in the dilepton mode.

The fatjets in the signal processes primarily originate from W/Z decays, with the leading fatjet mass peaking around their masses. Consequently, applying a window-like cut around this peak can effectively reduce back-

ground contributions. However, the fatjet mass distribution for the signal exhibits a bimodal nature, with a second peak appearing at the RHN mass. Due to this characteristic, we refrain from imposing a cut on the fatjet mass in our analysis.

IV. HL-LHC PROSPECTS

For the HL-LHC (14 TeV centre-of-mass energy with $\mathcal{L} = 3 \text{ ab}^{-1}$ of integrated luminosity), we estimate the number of signal events (N_S) and number of total background events (N_B) surviving the cuts listed in Table III. The N_S is calculated as,

$$N_S = \left(\sigma_{PP} \cdot \varepsilon_{PP} + \lambda^2 \cdot \sigma_{SP} \cdot \varepsilon_{SP} + \lambda^4 \cdot \sigma_{IP} \cdot \varepsilon_{IP} \right) \cdot \mathcal{L}, \quad (2)$$

where σ_{XX} and ε_{XX} ($XX = PP, SP, IP$) are the cross sections and efficiencies of the different signal processes. Here, λ represents the LQ coupling (x for sLQs and y for vLQs). Both σ and ε are functions of M_{ℓ_q} and M_{ν_R} , making N_S a function of these masses and λ . To determine the signal sensitivity, we use the following \mathcal{Z} -score [74] formula:

$$\mathcal{Z} = \sqrt{2(N_S + N_B) \ln \left(\frac{N_S + N_B}{N_B} \right)} - 2N_S. \quad (3)$$

The results for the monoelectron and dielectron final states are presented in Fig. 4, showing 2σ (\sim exclusion) and 5σ (discovery) contours in the $M_{\ell_q} - x(y)$ plane for sLQs (vLQs). For these plots, we set the benchmark RHN mass at 500 GeV. The dielectron channel offers stricter exclusions than the monoelectron channel because a cut on the dielectron invariant mass can significantly suppress the dominant Drell-Yan background. In Fig. 5, we show similar contours on the $M_{\ell_q} - M_{\nu_R}$ plane for $\lambda = 1$ in the dielectron channel. With increasing M_{ν_R} , the contours first bulge towards higher M_{ℓ_q} values till about $M_{\nu_R} = 500$ GeV and then return towards lower M_{ℓ_q} values. This happens because the selection efficiencies start low at low M_{ν_R} values and increase till about $M_{\nu_R} = 500$ GeV, where the cuts are optimised. Beyond this point, the efficiencies plateau, causing the contours to move towards smaller M_{ℓ_q} values as expected. The exclusion limits for vLQs are largely insensitive to κ , as the dominant contribution arises from the IP process, which is independent of κ . Although PP and SP depend on κ , their overall impact is relatively smaller. Consequently, for larger LQ masses where the IP process dominates, the effect of κ on limits remains negligible. The model-independent mass limits (from PP with $x \rightarrow 0$) for different vLQs for $\kappa = 0, 1$ are presented in Table V. (Note that since we optimise the cuts for the IP process, we obtain slightly less stringent model-independent mass limits than those obtained in Ref. [20].)

V. SUMMARY AND CONCLUSIONS

We investigated RHN productions at the LHC mediated by first-generation LQs and demonstrated the importance of

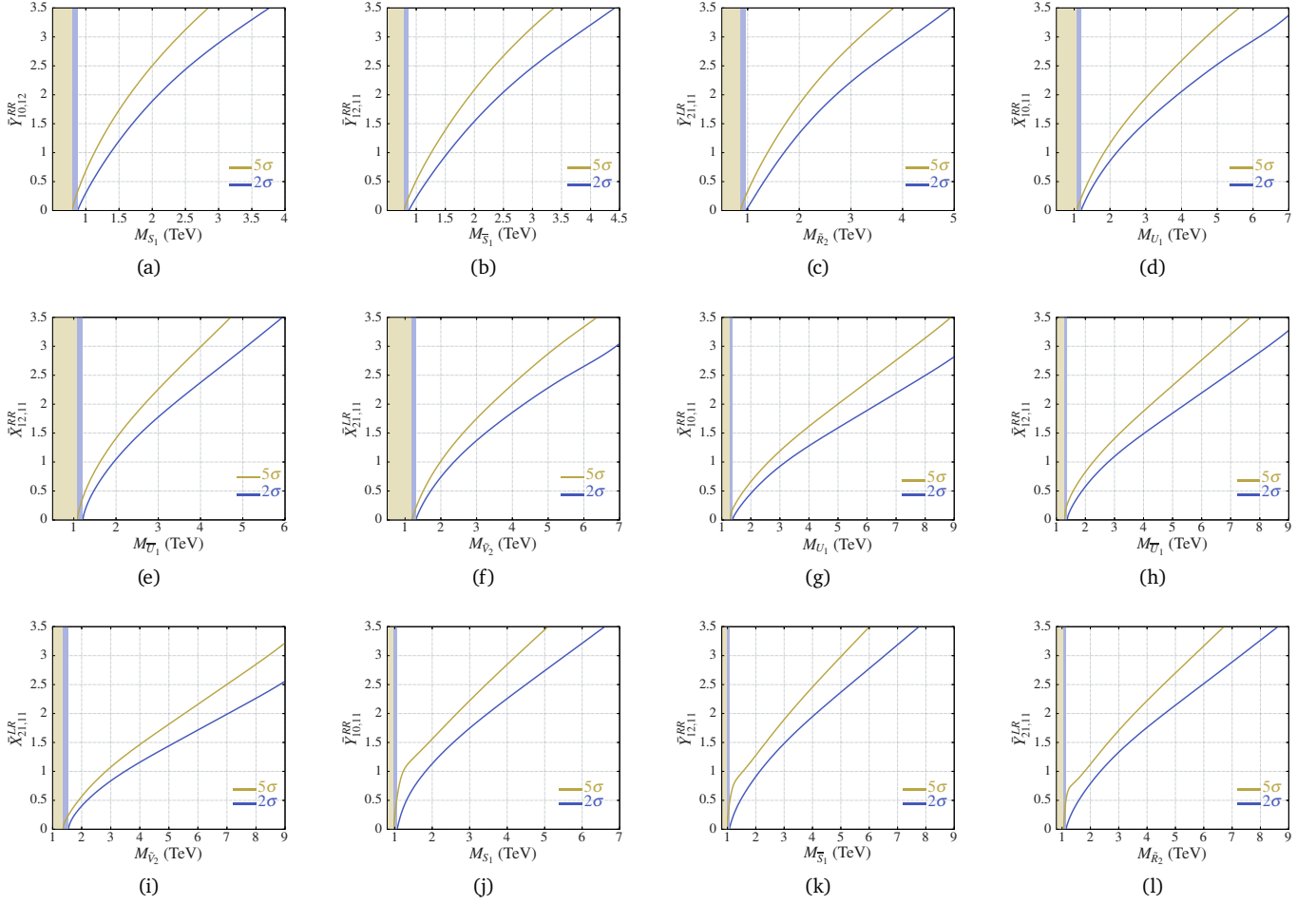


FIG. 4. The 2σ (exclusion) and 5σ (discovery) regions for sLQs and vLQs at the HL-LHC: [(a) – (f)] for mono-electron final states and [(g) – (l)] for dielectron final states. The vertical shaded regions indicate the model-independent limits (i.e., obtained only with PP by setting $x/y \rightarrow 0$) for different LQs. All these limits are obtained for $M_{V_R} = 500$ GeV. We set $\kappa = 1$ in the vLQ plots.

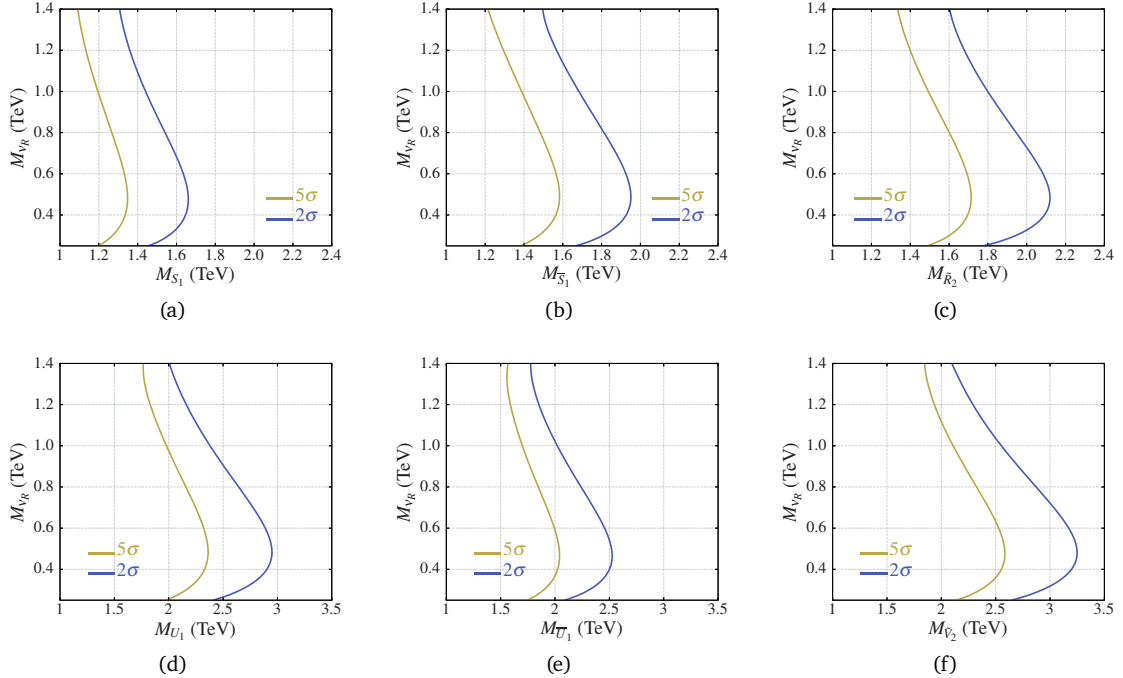


FIG. 5. The 2σ and 5σ regions for the dielectron final states on the $M_{lq} - M_{V_R}$ planes with fixed coupling, $x/y = 1$.

the t -channel LQ exchange process in this case. The first-generation process shows more promise at the HL-LHC than the second-generation one [20] because the larger quark PDFs significantly boost this process. We designed a set of criteria/cuts optimised for this channel. Though the cuts are less stringent than those used earlier in the second-generation case [20], the enhanced cross-sections result in stricter exclusion limits.

We estimated the projected HL-LHC exclusion limits and discovery reaches for all first-generation scalar and vector LQs that can produce a pair of RHNs decaying to produce monoelectron and dielectron final states. Due to reduced backgrounds, the dielectron channel shows better prospects than the monoelectron mode. However, both channels show good promise at the HL-LHC. If the LQ-RHN-quark coupling is large, the HL-LHC can probe LQ

masses between 3–10 TeV (depending on the type of the LQ) for a sub-TeV RHN. In the future, machine learning techniques can enhance the prospects even further. While the model-independent mass limits derived from the pair production of vector LQs depend on the choice of the κ parameter, the model-dependent limits are only marginally affected by κ , as the t -channel LQ exchange process essentially determines them as long as the new coupling controlling it is not very small.

ACKNOWLEDGEMENT

T.M. acknowledges partial support from the SERB/ANRF, Government of India, through the Core Research Grant (CRG) No. CRG/2023/007031. R.S. acknowledges the PMRF (ID: 0802000) from the Government of India.

-
- [1] P. Minkowski, $\mu \rightarrow e\gamma$ at a Rate of One Out of 10^9 Muon Decays?, *Phys. Lett. B* **67** (1977) 421–428.
- [2] R. N. Mohapatra and G. Senjanovic, *Neutrino Mass and Spontaneous Parity Nonconservation*, *Phys. Rev. Lett.* **44** (1980) 912.
- [3] R. N. Mohapatra, *Mechanism for Understanding Small Neutrino Mass in Superstring Theories*, *Phys. Rev. Lett.* **56** (1986) 561–563.
- [4] R. N. Mohapatra and J. W. F. Valle, *Neutrino Mass and Baryon Number Nonconservation in Superstring Models*, *Phys. Rev. D* **34** (1986) 1642.
- [5] A. M. Abdullahi et al., *The present and future status of heavy neutral leptons*, *J. Phys. G* **50** (2023) 020501, [2203.08039].
- [6] S. Banerjee, P. S. B. Dev, A. Ibarra, T. Mandal and M. Mitra, *Prospects of Heavy Neutrino Searches at Future Lepton Colliders*, *Phys. Rev. D* **92** (2015) 075002, [1503.05491].
- [7] A. Das, P. S. B. Dev and R. N. Mohapatra, *Same Sign versus Opposite Sign Dileptons as a Probe of Low Scale Seesaw Mechanisms*, *Phys. Rev. D* **97** (2018) 015018, [1709.06553].
- [8] W.-Y. Keung and G. Senjanovic, *Majorana Neutrinos and the Production of the Right-handed Charged Gauge Boson*, *Phys. Rev. Lett.* **50** (1983) 1427.
- [9] M. Thomas Arun, T. Mandal, S. Mitra, A. Mukherjee, L. Priya and A. Sampath, *Testing left-right symmetry with an inverse seesaw mechanism at the LHC*, *Phys. Rev. D* **105** (2022) 115007, [2109.09585].
- [10] A. Ekstedt, R. Enberg, G. Ingelman, J. Löfgren and T. Mandal, *Constraining minimal anomaly free $U(1)$ extensions of the Standard Model*, *JHEP* **11** (2016) 071, [1605.04855].
- [11] A. Das, N. Okada and D. Raut, *Enhanced pair production of heavy Majorana neutrinos at the LHC*, *Phys. Rev. D* **97** (2018) 115023, [1710.03377].
- [12] A. Das, N. Okada and D. Raut, *Heavy Majorana neutrino pair productions at the LHC in minimal $U(1)$ extended Standard Model*, *Eur. Phys. J. C* **78** (2018) 696, [1711.09896].
- [13] P. Cox, C. Han and T. T. Yanagida, *LHC Search for Right-handed Neutrinos in Z' Models*, *JHEP* **01** (2018) 037, [1707.04532].
- [14] A. Das, N. Okada, S. Okada and D. Raut, *Probing the seesaw mechanism at the 250 GeV ILC*, *Phys. Lett. B* **797** (2019) 134849, [1812.11931].
- [15] D. Choudhury, K. Deka, T. Mandal and S. Sadhukhan, *Neutrino and Z' phenomenology in an anomaly-free $U(1)$ extension: role of higher-dimensional operators*, *JHEP* **06** (2020) 111, [2002.02349].
- [16] K. Deka, T. Mandal, A. Mukherjee and S. Sadhukhan, *Leptogenesis in an anomaly-free $U(1)$ extension with higher-dimensional operators*, *Nucl. Phys. B* **991** (2023) 116213, [2105.15088].
- [17] A. Das, S. Mandal, T. Nomura and S. Shil, *Heavy Majorana neutrino pair production from Z' at hadron and lepton colliders*, *Phys. Rev. D* **105** (2022) 095031, [2202.13358].
- [18] M. T. Arun, A. Chatterjee, T. Mandal, S. Mitra, A. Mukherjee and K. Nivedita, *Search for the Z' boson decaying to a right-handed neutrino pair in leptophobic $U(1)$ models*, *Phys. Rev. D* **106** (2022) 095035, [2204.02949].
- [19] J. L. Evans and N. Nagata, *Signatures of Leptoquarks at the LHC and Right-handed Neutrinos*, *Phys. Rev. D* **92** (2015) 015022, [1505.00513].
- [20] A. Bhaskar, Y. Chaurasia, K. Deka, T. Mandal, S. Mitra and A. Mukherjee, *Right-handed neutrino pair production via second-generation leptoquarks*, *Phys. Lett. B* **843** (2023) 138039, [2301.11889].
- [21] J. C. Pati and A. Salam, *Unified Lepton-Hadron Symmetry and a Gauge Theory of the Basic Interactions*, *Phys. Rev. D* **8** (1973) 1240–1251.
- [22] J. C. Pati and A. Salam, *Lepton Number as the Fourth Color*, *Phys. Rev. D* **10** (1974) 275–289. [Erratum: *Phys.Rev.D* **11**, 703–703 (1975)].
- [23] H. Georgi and S. L. Glashow, *Unity of All Elementary Particle Forces*, *Phys. Rev. Lett.* **32** (1974) 438–441.
- [24] H. Fritzsch and P. Minkowski, *Unified Interactions of Leptons and Hadrons*, *Annals Phys.* **93** (1975) 193–266.
- [25] B. Schrempp and F. Schrempp, *LIGHT LEPTOQUARKS*, *Phys. Lett. B* **153** (1985) 101–107.
- [26] M. Kohda, H. Sugiyama and K. Tsumura, *Lepton number violation at the LHC with leptoquark and diquark*, *Phys. Lett. B* **718** (2013) 1436–1440, [1210.5622].
- [27] S. Dimopoulos and L. Susskind, *Mass Without Scalars*, *Nucl. Phys. B* **155** (1979) 237–252.

- [28] E. Farhi and L. Susskind, *Technicolor*, *Phys. Rept.* **74** (1981) 277.
- [29] R. Barbier et al., *R-parity violating supersymmetry*, *Phys. Rept.* **420** (2005) 1–202, [[hep-ph/0406039](#)].
- [30] U. Aydemir, T. Mandal, S. Mitra and S. Munir, *An economical model for B-flavour and a_μ anomalies from SO(10) grand unification*, [2209.04705](#).
- [31] A. Bhaskar, A. A. Madathil, T. Mandal and S. Mitra, *Combined explanation of W-mass, muon g-2, $RK^{(*)}$ and $RD^{(*)}$ anomalies in a singlet-triplet scalar leptoquark model*, *Phys. Rev. D* **106** (2022) 115009, [[2204.09031](#)].
- [32] A. Bhaskar, D. Das, S. Kundu, A. A. Madathil, T. Mandal and S. Mitra, *Vector leptoquark contributions to lepton dipole moments*, [2408.11798](#).
- [33] T. Mandal, S. Mitra and S. Seth, *Single Productions of Colored Particles at the LHC: An Example with Scalar Leptoquarks*, *JHEP* **07** (2015) 028, [[1503.04689](#)].
- [34] A. Bhaskar, D. Das, B. De and S. Mitra, *Enhancing scalar productions with leptoquarks at the LHC*, *Phys. Rev. D* **102** (2020) 035002, [[2002.12571](#)].
- [35] P. Bandyopadhyay, A. Karan, R. Mandal and S. Parashar, *Distinguishing signatures of scalar leptoquarks at hadron and muon colliders*, *Eur. Phys. J. C* **82** (2022) 916, [[2108.06506](#)].
- [36] K. Cheung, T. T. Q. Nguyen and C. J. Ouseph, *Leptoquark search at the Forward Physics Facility*, *Phys. Rev. D* **108** (2023) 036014, [[2302.05461](#)].
- [37] A. Bhaskar and M. Mitra, *Boosted top quark inspired leptoquark searches at the muon collider*, [2409.15992](#).
- [38] A. Bhaskar, Y. Chaurasia, A. Das, A. Kumar, T. Mandal, S. Mitra et al., *ToolQit: Leptoquark Models and Limits*, [2412.19729](#).
- [39] A. Bhaskar, A. Das, T. Mandal, S. Mitra and R. Sharma, *Fresh look at the LHC limits on scalar leptoquarks*, *Phys. Rev. D* **109** (2024) 055018, [[2312.09855](#)].
- [40] I. Doršner, S. Fajfer, A. Greljo, J. F. Kamenik and N. Košnik, *Physics of leptoquarks in precision experiments and at particle colliders*, *Phys. Rept.* **641** (2016) 1–68, [[1603.04993](#)].
- [41] J. Blumlein, E. Boos and A. Kryukov, *Leptoquark pair production in hadronic interactions*, *Z. Phys. C* **76** (1997) 137–153, [[hep-ph/9610408](#)].
- [42] J. Blümlein and E. Boos, *Leptoquark production at high energy e^+e^- colliders*, *Nucl. Phys. B Proc. Suppl.* **37** (1994) 181–192.
- [43] A. Alloul, N. D. Christensen, C. Degrande, C. Duhr and B. Fuks, *FeynRules 2.0 - A complete toolbox for tree-level phenomenology*, *Comput. Phys. Commun.* **185** (2014) 2250–2300, [[1310.1921](#)].
- [44] J. Alwall, R. Frederix, S. Frixione, V. Hirschi, F. Maltoni, O. Mattelaer et al., *The automated computation of tree-level and next-to-leading order differential cross sections, and their matching to parton shower simulations*, *JHEP* **07** (2014) 079, [[1405.0301](#)].
- [45] **NNPDF** collaboration, R. D. Ball et al., *An open-source machine learning framework for global analyses of parton distributions*, *Eur. Phys. J. C* **81** (2021) 958, [[2109.02671](#)].
- [46] M. Kramer, T. Plehn, M. Spira and P. M. Zerwas, *Pair production of scalar leptoquarks at the CERN LHC*, *Phys. Rev. D* **71** (2005) 057503, [[hep-ph/0411038](#)].
- [47] T. Mandal, S. Mitra and S. Seth, *Pair Production of Scalar Leptoquarks at the LHC to NLO Parton Shower Accuracy*, *Phys. Rev. D* **93** (2016) 035018, [[1506.07369](#)].
- [48] C. Borschensky, B. Fuks, A. Kulesza and D. Schwartländer, *Scalar leptoquark pair production at hadron colliders*, *Phys. Rev. D* **101** (2020) 115017, [[2002.08971](#)].
- [49] C. Borschensky, B. Fuks, A. Kulesza and D. Schwartländer, *Scalar leptoquark pair production at the LHC: precision predictions in the era of flavour anomalies*, *JHEP* **02** (2022) 157, [[2108.11404](#)].
- [50] C. Borschensky, B. Fuks, A. Kulesza and D. Schwartländer, *Precision predictions for scalar leptoquark pair production at the LHC*, *PoS EPS-HEP2021* (2022) 637, [[2110.15324](#)].
- [51] C. Borschensky, B. Fuks, A. Jueid and A. Kulesza, *Scalar leptoquarks at the LHC and flavour anomalies: a comparison of pair-production modes at NLO-QCD*, *JHEP* **11** (2022) 006, [[2207.02879](#)].
- [52] C. Bierlich et al., *A comprehensive guide to the physics and usage of PYTHIA 8.3*, *SciPost Phys. Codeb.* **2022** (2022) 8, [[2203.11601](#)].
- [53] **DELPHES 3** collaboration, J. de Favereau, C. Delaere, P. Demin, A. Giammanco, V. Lemaître, A. Mertens et al., *DELPHES 3, A modular framework for fast simulation of a generic collider experiment*, *JHEP* **02** (2014) 057, [[1307.6346](#)].
- [54] M. Cacciari, G. P. Salam and G. Soyez, *FastJet User Manual*, *Eur. Phys. J. C* **72** (2012) 1896, [[1111.6097](#)].
- [55] M. Cacciari, G. P. Salam and G. Soyez, *The anti-k_t jet clustering algorithm*, *JHEP* **04** (2008) 063, [[0802.1189](#)].
- [56] S. Catani, L. Cieri, G. Ferrera, D. de Florian and M. Grazzini, *Vector boson production at hadron colliders: A fully exclusive qcd calculation at next-to-next-to-leading order*, *Phys. Rev. Lett.* **103** (Aug, 2009) 082001.
- [57] G. Balossini, G. Montagna, C. M. Carloni Calame, M. Moretti, O. Nicrosini, F. Piccinini et al., *Combination of electroweak and qcd corrections to single w production at the fermilab tevatron and the cern lhc*, *Journal of High Energy Physics* **2010** (Jan., 2010) .
- [58] J. M. Campbell, R. K. Ellis and C. Williams, *Vector boson pair production at the lhc*, *Journal of High Energy Physics* **2011** (July, 2011) .
- [59] N. Kidonakis, *Theoretical results for electroweak-boson and single-top production*, *PoS DIS2015* (2015) 170, [[1506.04072](#)].
- [60] C. Muselli, M. Bonvini, S. Forte, S. Marzani and G. Ridolfi, *Top Quark Pair Production beyond NNLO*, *JHEP* **08** (2015) 076, [[1505.02006](#)].
- [61] A. Kulesza, L. Motyka, D. Schwartländer, T. Stebel and V. Theeuwes, *Associated production of a top quark pair with a heavy electroweak gauge boson at NLO+NNLL accuracy*, *Eur. Phys. J. C* **79** (2019) 249, [[1812.08622](#)].
- [62] S. Chakdar, K. Ghosh, V. Hoang, P. Q. Hung and S. Nandi, *Search for electroweak-scale right-handed neutrinos and mirror charged leptons through like-sign dilepton signals*, *Phys. Rev. D* **95** (Jan, 2017) 015014.
- [63] J. N. Ng, A. de la Puente and B. W.-P. Pan, *Search for Heavy Right-Handed Neutrinos at the LHC and Beyond in the Same-Sign Same-Flavor Leptons Final State*, *JHEP* **12** (2015) 172, [[1505.01934](#)].
- [64] Z. Kang, P. Ko and J. Li, *New avenues to heavy right-handed neutrinos with pair production at hadronic colliders*, *Phys. Rev. D* **93** (Apr, 2016) 075037.
- [65] E. Accomando, L. Delle Rose, S. Moretti, E. Olaiya and C. H. Shepherd-Themistocleous, *Extra Higgs boson and Z' as portals to signatures of heavy neutrinos at the LHC*, *JHEP* **02** (2018) 109, [[1708.03650](#)].
- [66] J. C. Helo, H. Li, N. A. Neill, M. Ramsey-Musolf and J. C. Vasquez, *Probing neutrino Dirac mass in left-right symmetric models at the LHC and next generation colliders*, *Phys. Rev. D* **99** (2019) 055042, [[1812.01630](#)].

- [67] K. Huitu, S. Khalil, H. Okada and S. K. Rai, *Signatures for right-handed neutrinos at the large hadron collider*, *Phys. Rev. Lett.* **101** (Oct, 2008) 181802.
- [68] F. F. Deppisch, S. Kulkarni and W. Liu, *Heavy neutrino production via Z' at the lifetime frontier*, *Phys. Rev. D* **100** (Aug, 2019) 035005.
- [69] C.-W. Chiang, G. Cottin, A. Das and S. Mandal, *Displaced heavy neutrinos from Z' decays at the LHC*, *JHEP* **12** (2019) 070, [1908.09838].
- [70] A. Das, P. B. Dev and N. Okada, *Long-lived tev-scale right-handed neutrino production at the lhc in gauged $u(1)_x$ model*, *Physics Letters B* **799** (2019) 135052.
- [71] F. F. Deppisch, W. Liu and M. Mitra, *Long-lived Heavy Neutrinos from Higgs Decays*, *JHEP* **08** (2018) 181, [1804.04075].
- [72] W. Liu, J. Li, J. Li and H. Sun, *Testing the seesaw mechanisms via displaced right-handed neutrinos from a light scalar at the HL-LHC*, *Phys. Rev. D* **106** (2022) 015019, [2204.03819].
- [73] A. Bhardwaj, P. Konar, T. Mandal and S. Sadhukhan, *Probing the inert doublet model using jet substructure with a multivariate analysis*, *Phys. Rev. D* **100** (2019) 055040, [1905.04195].
- [74] G. Cowan, K. Cranmer, E. Gross and O. Vitells, *Asymptotic formulae for likelihood-based tests of new physics*, *Eur. Phys. J. C* **71** (2011) 1554, [1007.1727]. [Erratum: *Eur.Phys.J.C* **73**, 2501 (2013)].